Journal of Materials Chemistry C

PAPER

Self-powered organolead halide perovskite single crystal photodetector driven by a DVD-based triboelectric nanogenerator†

Received 00th January 20xx,
Accepted 00th January 20xx

DOI: 10.1039/x0xx00000x

www.rsc.org/

Huajing Fang,[a] Qiang Li,[a] Jie Ding,[a] Nan Li,[a] He Tian,[b] Lijing Zhang,[a] Tianling Ren,[b] Jiyan Dai,[c] Liduo Wang,[a] and Qingfen Yan*[a]

Organolead halide perovskites have attracted extensive attentions as light harvesting materials for optoelectronic devices due to their high charge carrier mobility, high photoconversion efficiency, and long charge diffusion length. In this study, we present the first self-powered organolead halide perovskite single crystal photodetector driven by a triboelectric nanogenerator (TENG). A high-performance planar photodetector showing a responsivity of 7.92 A/W to white light under a bias of 4 V was fabricated on the (100) facet of a bulk $CH_3NH_3PbI_3$ perovskite single crystal. Furthermore, we demonstrate a cost-effective approach to the fabrication of a drum-shaped TENG by using two used digital versatile discs (DVDs), which could generate a high output of up to 200 V and 55 μA. By integrating the $CH_3NH_3PbI_3$ single crystal photodetector with the TENG, the self-powered device exhibited a large responsivity of 196 V/mW•cm^{-2} and a wide detection range from 10 μW/cm^2 to 100 mW/cm^2. These results prove a new strategy for driving the organolead halide perovskite photodetector with the energy harvested from the environment rather than external power supply.

1. Introduction

Photodetectors that can convert light into an electrical signal are crucial for various applications such as laser related sensor networks, imaging techniques, optical communications and many more.[1-5] Semiconductor materials are essential in this case for the generation of electron-hole (e-h) pairs via absorption of incident photons. Various types of semiconductor materials such as Si, ZnO, two-dimensional (2D) materials (MoS_2, GaTe, etc.), quantum dots and conjugated polymers have been applied in photodetectors.[6-11] Recently, organolead halide perovskites with a typical formula of $CH_3NH_3PbX_3$ (X=I, Br, or Cl) have emerged as a perfect candidate in the optoelectronic field. Great progress has been achieved on organolead halide perovskite solar cell in the past several years. The improvements on device structure and fabrication technique have enabled an overall power conversion efficiency over 20%.[12] Thanks to the excellent intrinsic optoelectronic properties, the emerging perovskite materials also demonstrated outstanding performance in photodetector. For instance, Hu et al.[13] reported the first organolead halide perovskite based photodetector with responsivity of 3.49 A/W, 0.0367 A/W at 365 nm and 780 nm, respectively. Lee and co-workers[14] demonstrated a hybrid photodetector with an enhanced responsivity as high as 180 A/W by introducing graphene to improve the efficient charge transfer. Very recently, Fang et al.[15] demonstrated a highly sensitive perovskite photodetector which could directly measure the weak light of sub 1 pW/cm^2 through the interfacial electron transfer layer (ETL) and hole transfer layer (HTL) engineering. In addition to these $CH_3NH_3PbX_3$ polycrystalline films photodetectors, the photodetectors based on organolead halide perovskite bulk single crystals have also been reported very recently. [16,17]

Generally, all the reported perovskite photodetectors can be mainly divided into two classes. One type of the photodetectors works by exploiting the photovoltaic effect.[15,18-21] These photodetectors can not only detect the signals but also be powered by the detected signals. The photogenerated e-h pairs are usually separated by the built-in potential difference provided by the junction-based multi-layer structures, which often involve complicated, time-consuming and uneconomic device fabrication process.[19] More importantly, material choice of this kind of devices is limited due to issues such as lattice mismatch, surface states and band alignment. The other type is the conventional photoconductive photodetectors in a planar geometry (semiconducting film deposited over the lateral arranged electrodes).[13,14,22-28] The simple structure endows them a convenience to fabricate or integrate with other devices. However, these photoconductive photodetectors need to be driven by external power supply. This issue not only increases the system size but also greatly limits the mobility and independence.[29] In this regard, it is of paramount importance to build a self-powered photodetector system that operates independently, sustainably, and wirelessly.

Owing to their sufficient electrical output, triboelectric nanogenerators (TENGs) have been widely used in self-powered

[a] Department of Chemistry, Tsinghua University, Beijing, 100084, China. E-mail: yanqf@mail.tsinghua.edu.cn (Q. Yan)
[b] Institute of Microelectronics, Tsinghua University, Beijing 100084, China.
[c] Department of Applied Physics, The Hong Kong Polytechnic University, Hong Kong, China.

†Electronic Supplementary Information (ESI) available. See DOI: 10.1039/x0xx00000x

systems such as chemical sensors,[30] UV sensors,[31] biosensors,[32] and magnetic sensor.[33] As an energy transferrer, TENG can convert mechanic energy into electric by a conjunction of triboelectrification and electrostatic induction.[34-36] However, a wider adoption of TENG in sensor field may be shadowed by the imperfect repeatability. In general, the randomness of external mechanical force usually results in nonuniform output peak values of the TENG, which restricts the fine quantitative study of each kind of sensors. Furthermore, to enhance the performance of TENGs, the surface morphologies of the friction layers were usually modified by the complex micro and nano processing technology such as photolithography,[37] dry-etching,[38] block copolymer self-assembly.[39] Most of these methods rely on expensive equipments and are difficult for mass production, hindering the popularity of TENG in self-powered systems.

In this work, we demonstrate a self-powered photoconductive photodetector based on $CH_3NH_3PbI_3$ perovskite single crystal. Single crystalline $CH_3NH_3PbI_3$ affords the planar-type photodetector a high sensitivity of 7.92 A/W to white light at a bias of 4 V. To break the stranglehold of the external power supply for such a photoconductive photodetector, we have configured a well-designed TENG to drive it. Through a periodic impact on the TENG by finger tapping, a high responsivity of 196 V/mW•cm^{-2} coupled with a wide detection range from 10 μW/cm^2 to 100 mW/cm^2 can be obtained. The TENG has a new and simple drum-shaped structure and is consisting of two used digital versatile discs (DVDs). Thus, it can be achieved through a very simple process which overcomes the limitations such as expensive instruments, high operating cost, as well as complex procedures in fabrication of TENG. This smart integrated module shows great potential as a self-powered photoconductive photodetector because it is directly driven by the energy harvested from its working environment rather than bulky batteries or power cables.

2. Experimental

2.1 Crystal growth and fabrication of photodetector

The $CH_3NH_3PbI_3$ single crystals were grown by a simple solution-processed method.[40] Briefly, $Pb(Ac)_2(H_2O)_3$ (99.5%, Sinoreagent) was dissolved in HI (57 wt% aqueous solution, Acros Organics) to get a clear yellow PbI_2 solution. CH_3NH_3I was prepared by neutralizing equimolar amounts of CH_3NH_2 (40 wt% aqueous solution, Aladdin) and HI. Then, the homogenous mixture of PbI_2 and CH_3NH_3I solution was transferred to an oven. Black crystals were attained during the slowly cooling down to room temperature. To fabricate the planar photodetector, $CH_3NH_3PbI_3$ perovskite single crystal was thinned and polished along (100) direction to ~1 mm thick using a mechanical method. The polished $CH_3NH_3PbI_3$ crystal was pasted on a glass slide as a holder. Then, a pair of Au electrodes with a channel of 60 μm in length and 1mm in width were deposited on the top surface by thermal evaporation through a shadow mask.

2.2 Fabrication of DVD-based TENG

Polycarbonate (PC) substrates were detached from used commercially available DVDs, due to their low cost and ready availability. After soaking in 2 mol/L NaOH (Sinopharm) and 2 mol/L HNO_3 (Sinopharm) for several hours, the metal coating layer in the DVD was fully dissolved. Then, the protective layer can be easily peeled off from the DVD. The PC substrate was rinsed with ethanol (99.95%, Sinopharm) to remove the residual organic dye. No chemical modification was needed for this nano-patterned face used as the friction layer of the TENG. Al conductive tape was stuck to the reverse side as electrode. A sanded Cu conductive tape was stuck to another DVD as the opposite friction layer. Finally, four pieces of PET were used to connect the two friction layers face to face, resulting in a drum-shaped TENG.

2.3 Characterization of materials and devices

The crystal structure of the $CH_3NH_3PbI_3$ single crystal was characterized by X-ray diffraction (XRD, Bruker D8-Advance) using Cu Kα radiation. PL spectra were collected by confocal Raman microscopic systems (Renishaw) with a 514 nm laser. The surface morphology of the roughened Cu electrode was observed by field-emission scanning electron microscopy (FESEM, JEOL JSM-6335F). The nanostructure of the PC substrates detached from a used DVD was imaged with an atomic force microscopy (AFM, Veeco Nanoscope V) in tapping mode. The current-voltage (I-V) and photodetection properties of the $CH_3NH_3PbI_3$ single crystal photodetector were measured using an electrochemical workstation (ZAHNER CIMPS) and a digital sourcemeter (Keithley 2400) under dark and illuminated conditions. A solar simulator (xenon lamp, Oriel, AM 1.5G light) and optical attenuators were used for adjustable illumination. The output voltage and current of the DVD-based triboelectric nanogenerator were measured by a digital multimeter (RIGOL DM3068). The self-powered photodetector measurement was performed by connecting the $CH_3NH_3PbI_3$ and TENG in a designed circuit. With the continuous finger tapping on the TENG, the dividing voltage on the $CH_3NH_3PbI_3$ was measured by the digital multimeter (RIGOL DM3068) as a function of light intensity.

3. Results and discussion

The single crystal of $CH_3NH_3PbI_3$ was grown by a method similar to the reported solution crystallization process.[40] Fig. 1a shows the powder XRD pattern of the ground crystals. All the diffraction peaks can be assigned to a perovskite structure with high purity and good quility.[41] The inset in Fig. 1a illustrates the resulting $CH_3NH_3PbI_3$ bulk crystal with the oriented natural (100) facet labelled. The photoluminescence (PL) spectrum of this $CH_3NH_3PbI_3$ single crystal is demonstrated in Fig. 1b. The photoluminescence peak position is located at 775 nm, in a good agreement with the value of this semiconductor reported earlier.[42]

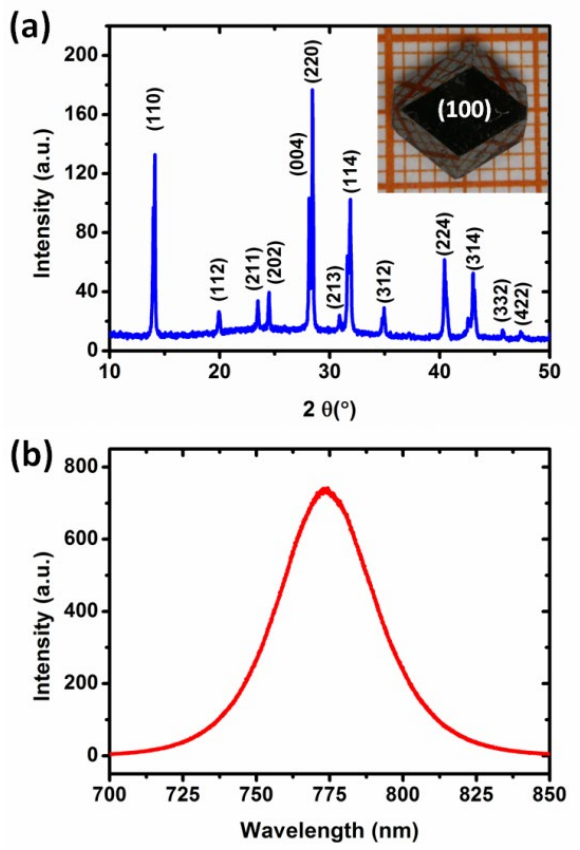

Fig. 1 (a) XRD patterns of the powders of the as-grown $CH_3NH_3PbI_3$ crystals. Inset shows the photograph of the obtained crystals (dimensions ~6 × 9 × 10 mm). (b) Photoluminescence (PL) spectrum of the $CH_3NH_3PbI_3$ single crystal upon excitation at 514 nm.

The $CH_3NH_3PbI_3$ perovskite single crystal was further processed to fabricate the photodetector with the simplest planar structure as schematically shown in Fig. 2a. To characterize the photodetector, we used a solar simulator coupled with optical attenuators as the white light source. Fig. 2b and c show the typical current-voltage (I-V) curves of the perovskite photodetector in the dark and illuminated with various intensities from 100 mW/cm^2 to 10 μW/cm^2. In order to make a clear contrast between the dark current and photocurrent under weak light, the I-V curves in Fig. 2c are plotted in a semi-log scale. It is apparent that, the photocurrent (I_{ph}) increases with the increase of light intensity (P), being consistent with the fact that more e-h pairs are excited by the increase of photon flux density. The corresponding dependence can be well fitted by a power law, $I_{ph} \sim P^{\beta}$, where β is a factor determines the response of the photocurrent to intensity. As plotted in Fig. 2d, the fitting gives a linear behavior with β = 0.66. This non-unity exponent (0.5 < β < 1) was due to the complex process of e-h pairs generation, recombination and trapping in $CH_3NH_3PbI_3$.[43,44] The responsivity R is a key parameter for photodetectors, and can be expressed as the the following equation:

$$R = \frac{I_{ph}}{P \times S}$$

where S is the effective area. It can be seen from Fig. 2d that the obtained responsivity also shows a linear relationship with the light intensity. Importantly, a high photoresponsivity of 7.92 A/W is observed in our device which is much higher than the values reported in polycrystalline film devices under the same light intensity (3.49 A/W).[13] The enhancement is derived from the presence of much less defects in single crystalline $CH_3NH_3PbI_3$. The elimination of grain boundaries and defects in the carrier transport direction can reduce charge recombination and improve the carrier diffusion length. For a given semiconductor applied in photodetector, the carrier diffusion length determines how efficient the photogenerated free charges can be collected by the electrode. Recently, a surprisingly long carrier diffusion length of > 175 μm has been reported in the $CH_3NH_3PbI_3$ single crystals, which is several orders of magnitude higher than the value in polycrystalline film.[45]

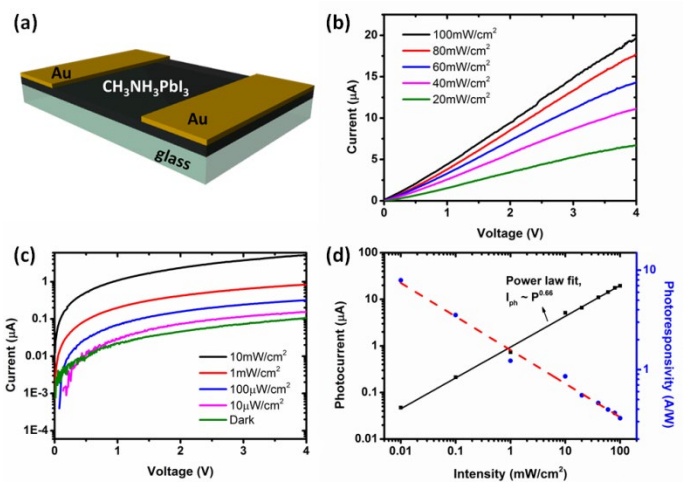

Fig. 2 (a) Schematic diagram of the perovskite photodetector based on $CH_3NH_3PbI_3$ single crystal (Au electrodes with a channel of 60 μm in length and 1mm in width). Photocurrent versus voltage plots (I-V curves) of the photodetector in the dark and under different white light illumination intensities (b) from 100 to 20 mW/cm^2 and (c) from 10 mW/cm^2 to 10 μW/cm^2, plotted on the semi-logarithmic scale. (d) Photocurrent and photoresponsivity as a function of illumination intensity at a bias of 4 V.

Next, we characterized the photoresponse switching behavior in order to clarify the robustness and reproducibility of this perovskite photodetector. As shown in Fig. 3a, the channel current as a function of time was measured during periodically switching of 100 mW/cm^2 light illumination. More than a dozen switching cycles was performed at a bias of 4 V. The photodetector exhibited good on-off switching with current ratio around 130. Response time is another important parameter of a photodetector. It can be seen from the enlarged view of a single on-off cycle (Fig. 3b), both the rise and decay time (t_r and t_d) are smaller than 0.2 s, acquiring the exact values of which is limited by the detection limit of our measurement system.

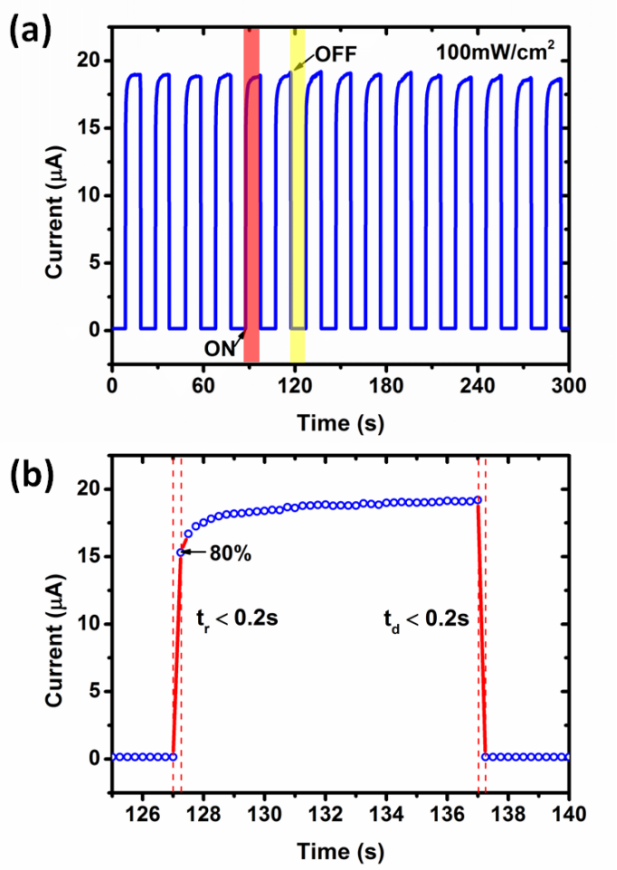

Fig. 3 Time response of the $CH_3NH_3PbI_3$ perovskite photodetector. (a) Photoresponses of the device upon 100 mW/cm^2 white light illumination at a bias of 4 V. (b) Enlarged view of a single cycle photocurrent response during on-off illumination switching.

The above results indicate that the $CH_3NH_3PbI_3$ single crystal photodetector can achieve a satisfactory performance with the simplest planar geometry. However, all the electrical signals of this photodetector were driven by the external bias. While self-powered nanosystems have gradually become the most desirable and promising prototype for environmental detection in these years because no battery is needed to power the device. Bearing this in mind, we paid our attention to the triboelectric nanogenerators, which have emerged as a rising star in the field of self-powered nanosystems. As for this power generation unit, a potential is first created between two materials that have opposite tribo-polarity due to the charge transfer caused by triboelectric effect. Then, in the outer circuit, electrons are driven to flow between two electrodes attached on the generator in order to balance the potential.[34] Previous works have demonstrated that micro/nanostructures existing on the surface of friction layers could contribute to higher performance of a TENG.[35] However, the fabrication of most of these micro/nanostructures relies on the expensive equipment, complex procedures, etc. It is well known that the used DVD in our daily life possesses a ready-made nanopatterned surface. Although it has been successfully used as a low-cost and environmentally friendly nanoimprint mold,[46] their application in the field of TENG has rarely been reported. To take advantage of the fine nanostructures on the DVD surface, we designed a novel TENG made from two used DVDs. Fig. 4a schematically illuminates the drum-shaped structure of this TENG. The polycarbonate (PC) substrate with nanopatterned surface detached from a used DVD and a rough Cu conductive tape sticking on the other used DVD were chosen as the opposite friction layers. The pressing and releasing cycles of this drum-shaped TENG can be easily realized based on the elasticity of polyethylene terephthalate (PET) connector distributed in four directions. The detailed working principle was depicted in Fig. S1 in the Supporting Information. Fig. 4b displays a photograph of the transparent PC substrate detached from a used DVD. Fig. 4c is the corresponding AFM image scanned from an arbitrary area in the PC substrate. In the scanned area of 15 μm × 15 μm, several DVD pits with a depth of about 200 nm can be observed. More detailed information of the pit sizes and their distances is analyzed in Fig. S2 in the Supporting Information. Furthermore, in order to enhance the performance of TENG, the Cu conductive tape was sanded before sticking to another used DVD as the opposite friction layer. Fig. 4d is the SEM image of the sanded Cu tape, revealing the micro/nano structured surface.

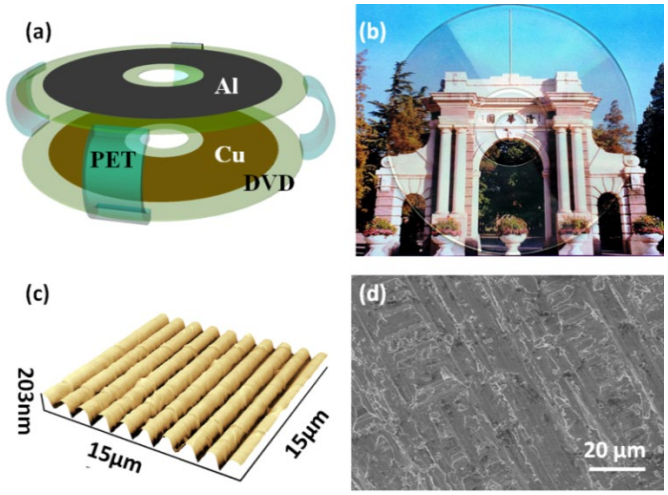

Fig. 4 (a) Schematic illustration of the drum-shaped TENG. (b) Photograph of the transparent PC substrate detached from a used DVD. (c) AFM image of the PC substrate with regular nanostructures. (d) SEM image of the Cu conductive tapes with rough surfaces.

We then investigated the output performance of this novel TENG under periodic deformation through finger tapping. As shown in Fig. 5a and b, the peak values of the open-circuit voltage and short-circuit current were found to be about 200 V and 55 μA, respectively. To verify that the measured signals were purely generated by the TENG, the widely used switching polarity test was also conducted for this DVD-based TENG (see Fig. S3 in the Supporting Information). Moreover, to visually present the generated electrical energy, 50 commercial green LEDs was directly turned on by finger tapping the TENG (see Video S1 in the Supporting Information).

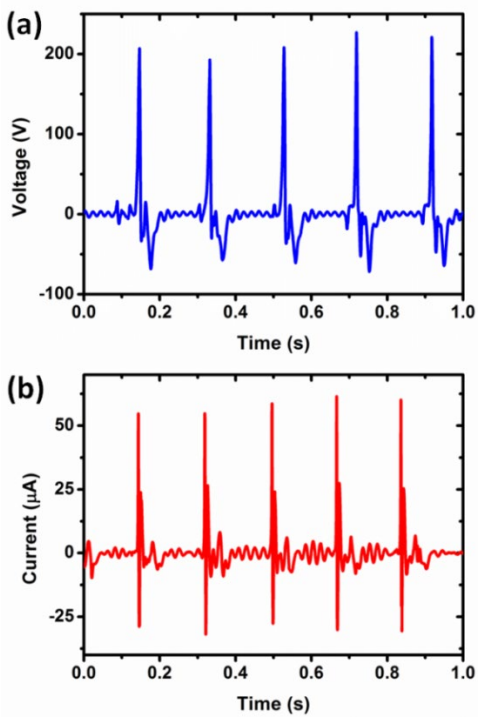

Fig. 5 Performance characterization of the TENG during the periodical finger tapping. The measured (a) open-circuit voltage and (b) short-circuit current signals in the forward connection.

The high performance of this DVD-based nanogenerator enables us to harvest energy from the working environment and directly drive the previously mentioned $CH_3NH_3PbI_3$ single crystal photodetector. However, because of the randomness of finger tapping, the peak value of obtained output voltage cannot keep as a constant (see Fig. 5a). This is a widespread problem which restricts the development of TENG in self-powered device, especially the quantitative sensors. With repeated compressive loading cycles produced by a linear motor to substitute the finger tapping to deform a nanogenerator was proved to be feasible previously,[30] but this method is not convenient in practical application. Here, we present a new approach to solve this problem by a unique circuit design. Fig. 6a shows the equivalent circuit of our self-powered photodetector nanosystem. A commercial Zener diode (1N4764A) was connected in parallel to the TENG as a voltage regulator. As known, the diode exhibits a controlled breakdown voltage and keeps the voltage drop close to the Zener breakdown voltage across a wide range of reverse currents. The regulated voltage after applying the Zener diode (see Fig. S4 in the Supporting Information) was used to drive the perovskite photodetector. Here, the photodetector behaves as a variable external load resistor which can be controlled by incident light. As expected, it was observed that the measured voltage drop across the $CH_3NH_3PbI_3$ single crystal photodetector changed as a function of the illumination intensity. In can be seen in Fig. 6b and c, the measured voltage decreases with increasing the illumination intensity. The change in voltage can be defined by $[(V_0\text{-}V)/V_0] \times 100\%$, where V_0 corresponds to the dark voltage and V corresponds to the measured voltage under different light illumination intensity. The dependence of the voltage change on the incident intensity shows an exponential relationship from 100 mW/cm^2 to 10 μW/cm^2 (Fig. 6d). The measuring principle set forth herein is different from that in conventional photoconductors, i.e., the detection signal is a voltage rather than a current. Therefore, photoresponsivity (R_v) of this nanosystem was defined as follows:

$$R_V = (V_0 - V)/P$$

where P corresponds to the incident light intensity. Fig. 6d shows the photoresponsivity as a function of light intensity, which can be fitted very well with $R_v \sim P^{0.59}$. The nanosystem exhibits a wide detection range from 10 μW/cm^2 to 100 mW/cm^2 and the largest responsivity of 196 V/mW•cm^{-2} at an illumination intensity of 10 μW/cm^2. Since the TENG can be easily driven wherever movement is available, the creative combination of TENG and the perovskite photodetector can works as a sustainable and wireless self-powered system.

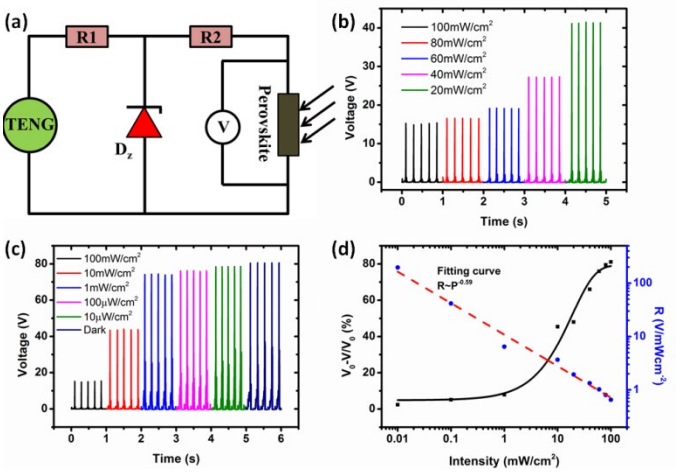

Fig. 6 (a) The equivalent circuit of the self-powered photodetector nanosystem. D_z represents a commercial Zener diode. (b, c) The measured voltage drop across the $CH_3NH_3PbI_3$ single crystal photodetector in the dark and under various illumination intensities. (d) Voltage change (defined as $(V_0\text{-}V)/V_0$) and photoresponsivity of the nanosystem as a function of illumination intensity.

4. Conclusions

In summary, we have demonstrated a self-powered planar photodetector based on $CH_3NH_3PbI_3$ single crystal. On the one hand, the excellent intrinsic optoelectronic properties of the single crystalline $CH_3NH_3PbI_3$ ensured the planar photodetector with a high responsivity of 7.92 A/W to white light under a bias of 4 V. On the other hand, an efficient TENG was made from two used DVDs generating an effective output of up to 200 V and 55 μA. By configuring such a TENG to the $CH_3NH_3PbI_3$ single crystal photodetector, a self-powered module was attained and it exhibited a high responsivity of 196 V/mW•cm^{-2} and a wide detection range from 10 μW/cm^2 to 100 mW/cm^2. It is also worth mentioning that the Zener diode has been introduced as a voltage regulator of TENG, which provides a universal method for easily and effectively improving the accuracy of self-powered device, especially for the

quantitative sensors. Our results might open up an avenue for the applications of organolead halide perovskite materials in self-powered optoelectronic devices.

Acknowledgements

This research was supported by the National key Basic Research Program of China (973 Program) under Grant No. 2013CB632900, the National Science Foundation of China (No. 51173097 and 91333109) and the Hong Kong Polytechnic University strategic project (No. 1-ZVCG). The Tsinghua University Initiative Scientific Research Program and the Open Research Fund Program of the State Key Laboratory of Low-Dimensional Quantum Physics (No. KF201516) are acknowledged for partial financial support.

References

1 L. F. Hu, M. M. Brewster, X. J. Xu, C. C. Tang, S. Gradecak and X. S. Fang, *Nano Lett.*, 2013, **12,** 1941-1947.
2 T. Y. Zhai, L. Li, X. Wang, X. S. Fang, Y. Bando and D. Golberg, *Adv. Funct. Mater.*, 2010**, 20**, 4233-4248.
3 Z. N. Wang, R. M. Yu, X. N. Wen, Y. Liu, C. F. Pan, W. Z. Wu and Z. L. Wang, *ACS Nano*, 2014**, 8,** 12866-12873.
4 S. Y. Lee, K. I. Park, C. Huh, M. Koo, H. G. Yoo, S. Kim, C. S. Ah, G. Y. Sung and K. J. Lee, *Nano Energy*, 2012**, 1,** 145-151.
5 X. S. Fang, L. M. Wu and L. F. Hu, *Adv. Mater.* **2011,** *23*, 585-598.
6 J. Michel, J. F. Liu and L. C. Kimerling, *Nat. Photonics* **2010,** *4*, 527-534.
7 A. A. Chaaya, M. Bechelany, S. Balme and P. Miele, *J. Mater. Chem. A*, 2014, **2,** 20650-20658.
8 D. S. Tsai, K. K. Liu, D. H. Lien, M. L. Tsai, C. F. Kang, C. A. Lin, L. J. Li and J. H. He, *ACS Nano*, 2013, **7,** 3905-3911.
9 F. Liu, H. Shimotani, H. Shang, T. Kanagasekaran, V.Zolyomi, N. Drummond, V. Falko and K. Tanigaki, *ACS Nano*, 2014**, 8**, 752-760.
10 J. P. Clifford, G. Konstantatos, K. W. Johnston, S. Hoogland, L. Levina and E. H. Sargent, *Nat. Nanotechnol.*, 2009**, 4**, 40-44.
11 H. L. Dong, H. F. Zhu, Q. Meng, X. Gong and W. P. Hu, *Chem. Soc. Rev.*, 2012**, 41**, 1754-1808.
12 Best Research-Cell Efficiency, http://www.nrel.gov/ncpv/images/efficiency_chart.jpg accessed: December 2014.
13 X. Hu, X. D. Zhang, L. Liang, J. Bao, S. Li, W. L. Yang and Y. Xie, *Adv. Funct. Mater.*, 2014**, 46**, 7373-7380.
14 Y. Lee, J. Kwon, E. Hwang, C. H. Ra, W. J. Yoo, J. H. Ahn, J. H. Park and J. H. Cho, *Adv. Mater.*, 2015**, 27,** 41-46.
15 Y. J. Fang and J. S. Huang, *Adv. Mater.*, 2015, **27**, 2804-2810.
16 Y. J. Fang, Q. F. Dong, Y. C. Shao, Y. B. Yuan and J. S. Huang, *Nat. Photon.*, 2015, **9,** 679-686.
17 G. Maculan, A. D. Sheikh, A. L. Abdelhady, M. I. Saidaminov, M. A. Haque, B. Murali, E. Alarousu, O. F. Mohammed, T. Wu and O. M. Bakr, *J. Phys. Chem. Lett.* 2015, 6, 3781-3786.
18 L. T. Dou, Y. Yang, J. B. You, Z. R. Hong, W. H. Chang, G. Li and Y. Yang, *Nat. Commun.*, 2014**, 5**, 5404.
19 D. Li, G. F. Dong, W. Z. Li and L. D. Wang, *Sci. Rep.*, 2015, **5,** 7902.
20 R. Dong, Y. J. Fang, J. Chae, J. Dai, Z. G. Xiao, Q. F. Dong, Y. B. Yuan, A. Centrone, X. C. Zeng and J. S. Huang, *Adv. Mater.*, 2015**, 27**, 1912-1918.
21 Q. Q. Lin, A. Armin, D. M. Lyons, P. L. Burn and P. Meredith, *Adv. Mater.*, 2015, **27,** 2060-2064.
22 E. Horváth, M. Spina, Z. Szekrényes, K. Kamarás, R. Gaal, D. Gachet and L. Forró, *Nano Lett.*, 2014, **14,** 6761-6766.
23 H. R. Xia, J. Li, W. T. Sun and L. M. Peng, *Chem. Commun.*, 2014**, 50**, 13695-13697.
24 Y. L. Guo, C. Liu, H. Tanaka and E. Nakamura, *J. Phys. Chem. Lett.*, 2015**, 6,** 535-539.
25 H. Deng, D. D. Dong, K. K. Qiao, L. L. Bu, B. Li, D. Yang, H. E. Wang, Y. B. Cheng, Z. X. Zhao, J. Tang and H. S. Song, *Nanoscale*, 2015, **7,** 4163-4170.
26 M. Spina, M. Lehmann, B. Náfrádi, L. Bernard, E. Bonvin, R. Gaál, A. Magrez, L. Forró and E. Horváth, *Small*, 2015, **11,** 4824-4828.
27 S. F. Zhuo, J. F. Zhang, Y. M. Shi, Y. Huang and B. Zhang, *Angew. Chem.*, 2015**, 127**, 5785-5788.
28 G. Walters, B. Sutherland, S. Hoogland, D. Shi, R. Comin, D. P. Sellan, O. M. Bakr and E. H. Sargent, *ACS Nano*, 2015**, 9,** 9340-9346.
29 L. Peng, L. F. Hu and X. S. Fang, *Adv. Funct. Mater.*, 2014**, 24,** 2591-2610.
30 Z. H. Lin, G. Zhu, Y. S. Zhou, Y. Yang, P. Bai, J. Chen and Z. L. Wang, *Angew. Chem. Int. Ed.*, 2013, **52,** 5065-5069.
31 Z. H. Lin, G. Cheng, Y. Yang, Y. S. Zhou, S. Lee and Z. L. Wang, *Adv. Funct. Mater.*, 2014**, 24,** 2810-2816.
32 H. L. Zhang, Y. Yang, T. C. Hou, Y. J. Su, C. G. Hu and Z. L. Wang, *Nano Energy*, 2013**, 2,** 1019-1024.
33 Y. Yang, L. Lin, Y. Zhang, Q. S. Jing, T. C. Hou and Z. L. Wang, *ACS Nano*, 2012, **6,** 10378-10383.
34 Z. L. Wang, *ACS Nano*, 2013, **7,** 9533-9557.
35 Q. Leng, H. Y. Guo, X. M. He, G. L. Liu, Y. Kang, C. G. Hu and Y. Xi, *J. Mater. Chem. A*, 2014, **2**, 19427-19434.
36 G. Liu, W. N. Xu, X. N. Xia, H. F. Shi and C. G. Hu, *J. Mater. Chem. A*, 2015, DOI: 10.1039/c5ta06438d.
37 S. H. Wang, L. Lin and Z. L. Wang, *Nano Lett.*, 2012, **12,** 6339-6346.
38 L. Lin, S. H. Wang, Y. N. Xie, Q. S. Jing, S. M. Niu, Y. F. Hu and Z. L. Wang, *Nano Lett.*, 2013**, 13,** 2916-2923.
39 C. K. Jeong, K. M. Baek, S. Niu, T. W. Nam, Y. H. Hur, D. Y. Park, G. T. Hwang, M. Byun, Z. L. Wang, Y. S. Jung and K. J. Lee, *Nano Lett.*, 2014**, 14,** 7031-7038.
40 Y. Y. Dang, Y. Liu, Y. X. Sun, D. S. Yuan, X. L. Liu, W. Q. Lu, G. F. Liu, H. B. Xia and X. T. Tao, *Cryst. Eng. Commun.*, 2015, **17,** 665-670.
41 M. I. Saidaminov, A. L. Abdelhady, B. Murali, E. Alarousu, V. M. Burlakov, W. Peng, I. Dursun, L. F. Wang, Y. He, G. Maculan, A. Goriely, T. Wu, O. F. Mohammed and O. M. Bakr, *Nat. Commun.*, 2015**, 6,** 7586.
42 B. W. Park, S. M. Jain, X. L. Zhang, A. Hagfeldt, G. Boschloo and T. Edvinsson, *ACS Nano*, 2015, **9,** 2088-2101.
43 H. Kind, H. Q. Yan, B. Messer, M. Law and P. D. Yang, *Adv. Mater.*, 2002, **14**, 158-160.
44 L. Li, P. S. Lee, C. Yan, T. Y. Zhai, X. S. Fang, M. Y. Liao, Y. Koide, Y. Bando and D. Golberg, *Adv. Mater.*, 2010**, 22**, 5145-5149.
45 Q. Dong, Y. Fang, Y. Shao, P. Mulligan, J. Qiu, L. Cao and J. S. Huang, *Science*, 2015**, 347,** 967-970.
46 J. R. Ell, T. A. Crosby, J. J. Peterson, K. R. Carter and J. J. Watkins, *Chem. Mater.*, 2010**, 22**, 1445-1451.

